

A Generalized FEM Model for Fiber Structural and Mechanical Performance in Fabrication of Slender Yarn Structures

Sheng Yan Li¹, Bin Gang Xu^{1,2}, Xiao Ming Tao¹ and Hong Hu¹

Abstract: Slender yarn structure made from natural fibers, nano-fibers, carbon nanotubes or other types of fibrous materials is all formed by twisting an assembly of short or long fibers and its performance is significantly influenced by the physical behavior of these fibers in the slender yarn forming region - a small triangle area called spinning triangle. In this paper, a new generalized FEM model of spinning triangle has been developed to theoretically analyze the fiber structural and mechanical performance in fabrication of these slender yarn structures. In this proposed model, a geometrical model of spinning triangle is developed and the initial conditions are formulated together with algorithms for fiber buckling. Compared with the earlier models, some important parameters ignored previously such as the inclined angle of spinning tension and fiber torsional strains are considered. Fiber tensions predicted by the model are in good agreements with earlier models while the predicted torque of slender yarns is generally more close to experimental measurements. In addition, the effect of the parameters neglected previously has also been fully analyzed by using the proposed FEM model.

Keywords: Finite Element Method, Fiber Tension, Fiber Torsion, Yarn Structure.

1 Introduction

Fiber and slender yarn are the fundamental materials for making a broad range of functional structures and textile composites such as geotextiles [Cartaud, Touze-Foltz and Duval, 2005], 3D auxetics and protectors [Liu, Hu, Lam and Liu, 2010; Miller, Hook, Smith, Wang and Evans, 2009], carbon nanotube and electro-spun polymer yarns [Jiang, Li and Fan, 2002; Smit, Buttner and Sanderson, 2005; Zakhidov, Nanjundaswamy, Obraztsov, Zhang, Fang, Klesch, Baughman and Zakhi-

¹ Institute of Textiles and Clothing, the Hong Kong Polytechnic University, Hung Hom, Kowloon, Hong Kong

² Corresponding author. E-mail address: tcxubg@inet.polyu.edu.hk

dov, 2007; Zhang, Atkinson and Baughman, 2004], and membranes [Oñate and Kröplin, 2005]. The property of constituent fibers, together with their spatial distribution inside the slender yarn, play an important role in determining the physical performance of yarns and their composites, such as the strength, internal torque and regularity [Hearle, Grosberg and Backer, 1969]. Spinning is a process which converts short or long fibers into a continuous yarn (see Fig. 1). For example, Fig. 2 shows the scanning electron microscope (SEM) images of a carbon nanotube (CNT) yarn being pulled out (by a tension) from a super-aligned CNT array grown on a silicon substrate [Zhang, Atkinson and Baughman, 2004]. The yarns could be further twisted into two or four-ply CNT threads, or formed into a more complicated knitted structure, as shown in Fig. 3.

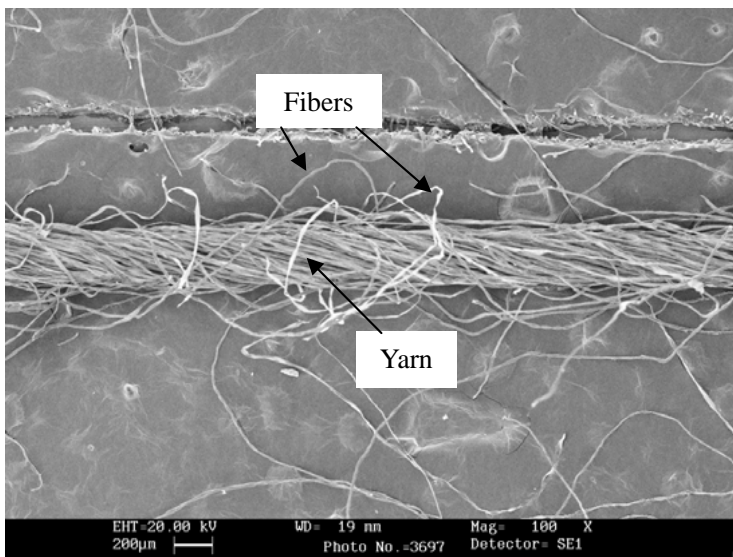


Figure 1: Scanning electron microscope (SEM) image of a yarn made by natural fibers

In the yarn fabrication process, the area between the front nip line (on the array) and the twisting point is called a twisting triangle or spinning triangle (see Fig. 2 and Fig. 4) where fibers will be eventually twisted into the yarn. Therefore the structural and physical properties of slender yarn will be greatly influenced by the geometric shape and the fiber mechanical behavior of the spinning triangle.

Over the past years, the investigation on yarn fabrication process or the spinning triangle has attracted an increasing interest of researchers and some valuable research works have been carried out [Fujino, Uno, Shiomi, Yanggawa and Kitada, 1962;

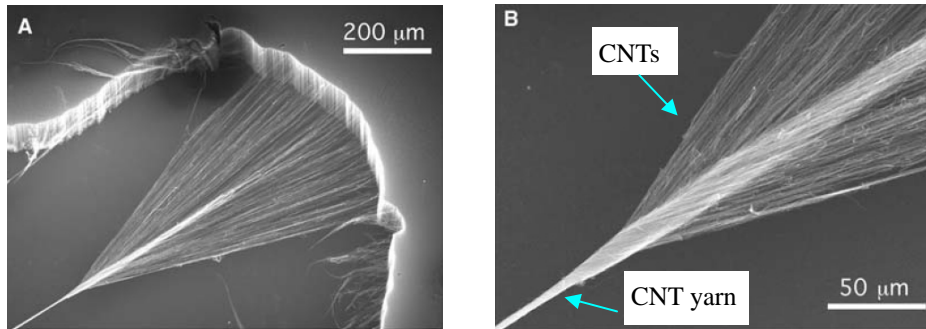


Figure 2: SEM images of (A) a carbon nanotube (CNT) yarn being pulled out and twisted from a nanotube array grown on a silicon substrate and (B) a magnified view of the spinning triangle of the CNT yarn [Zhang, Atkinson and Baughman, 2004]

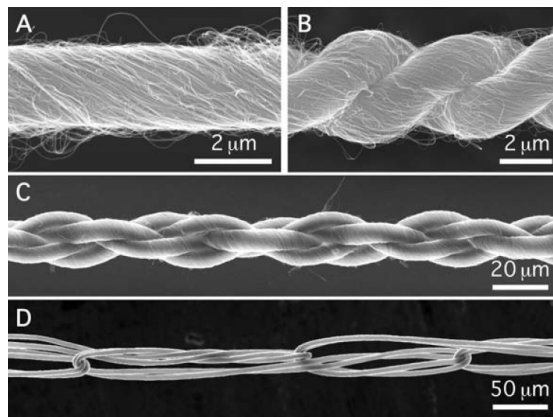


Figure 3: SEM images of a carbon nanotube: (A) single yarn, (B) two-ply yarn, (C) four-ply yarn and (D) knitted structure [Zhang, Atkinson and Baughman, 2004]

Pavlov, 1965; Krause, Soliman and Tian, 1991; El-Shiekh, 1965; Najjar, 1996; Hua, 2006; Hua, Tao, Cheng and Xu, 2007]. In the earlier stage of studies, the force method was the mainstream for the geometric and strength study of spinning triangle. For instance, Fujino, Uno, Shiomi, Yanggawa and Kitada (1962) examined the twist irregularity of yarns with a theoretical consideration of force balances in the spinning triangle. In a study of the fiber strength, structural transformations of the fibers at the instant rupture in yarn formation were studied by Pavlov (1965). Krause, Soliman and Tian (1991) also carried out a similar theoretical investigation

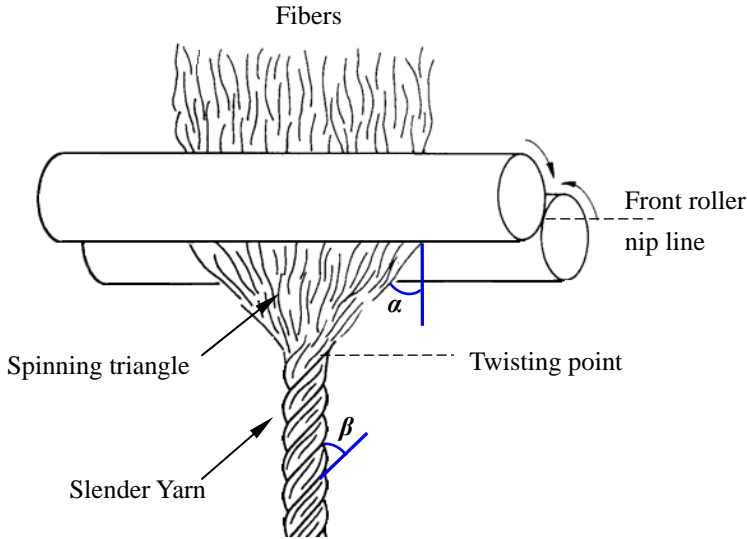


Figure 4: A sketch view of a symmetric spinning triangle. α is the half of spinning angle and β is the helix angle of the fiber distributed on the surface of the yarn.

on the strength of spinning triangle for yarns by taking different extensions of fiber into consideration. Based on the photographic experiments [El-Shiekh, 1965; Najjar, 1996; Hua, 2006], the behavior of fibers, such as fiber buckling, fiber migration and the profile of spinning triangle, were partially observed.

The theoretical models of spinning triangle currently in use were mainly based on the energy method. The advantage of this method lies that the full description of geometry is not required before hand. In those models [Najar, 1996; Hua, 2006; Hua, Tao, Cheng and Xu, 2007], the total potential energy, composed of the total elastic strain energy of fibers and the work done by the spinning tension, was minimized with respect to a generalized coordinate. Najjar (1996) originally carried out a theoretical study of the symmetric spinning triangle using the energy method. The distribution of fiber tensions in the symmetric spinning triangle was systematically studied with respect to its influencing parameters of twisting angle, spinning tension and yarn linear density. Hua (2006) and Hua, Tao, Cheng and Xu (2007) further extended the work of Najjar (1996) with the consideration of an asymmetric spinning triangle. Although the above-mentioned models are somehow capable of predicting fiber tension during yarn fabrication, because of the mathematical complexity in formulating fiber strains inside the spinning triangle, only the fiber tensile strain was considered and the spinning tension was assumed to be exactly vertical

to the front roller nip line of the spinning triangle (e.g. $\theta=0$ in Fig. 5). In addition, the fiber torsional strain was ignored due to the complexity.

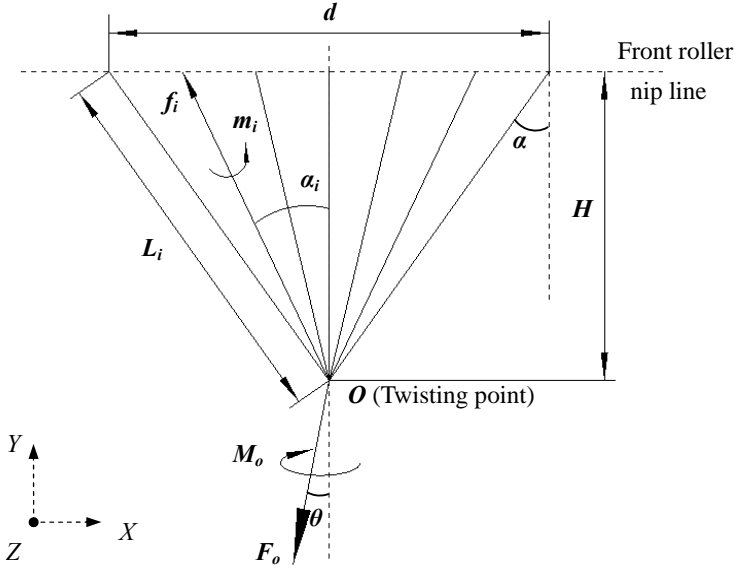


Figure 5: A geometric model of spinning triangle. d is the width of spinning triangle, H is the height of spinning triangle, f_i , m_i are the tension and elastic torque of i th fiber, respectively, α_i is the angle between the i th fiber and the vertical axis of front roller nip line, L_i is the length of i th fiber inside the spinning triangle, O is the twisting point, F_o is spinning tension, M_o is spinning torque, θ is the angle between the spinning tension of yarn and the vertical axis of front roller nip line and X , Y , Z are the global coordinates.

With the rapid development of computer technology, the Finite Element Method (FEM) becomes more widely used in analysis of textile structures. For instance, numerical simulations of fabric performance including the buckling analysis of knitted fabric [Zhang, Liu and Du, 2007], the impact analysis on a ballistic fabric [Duan, Keefe, Bogetti and Powers, 2006], drape simulation of woven fabric [Sze and Liu, 2007] and so on were carried out by using FEM. The FEM model of fabric material was built up for numerical simulating the behavior of fabric materials [Bouzidi, Ravaut and Wielgosz, 2003; Tanaka, Noguchi, Fujikawa, Sato, Oi, Kobayashi, Furuichi, Ishimaru and Nonomura, 2010; Wang, Zhang, Gao and Wang, 2007]. Another application is theoretical modeling of composite materials with textile reinforcement [Quek, Waas, Shahwan and Agaram, 2003; Sejnoha and

Zemana, 2008; Tabiei and Jiang, 1999].

In practice, the actual performance of the spinning triangle is more complicated than what have been modeled so far. For instance, the spinning tension of the yarn always has a large or small angle with the vertical axis of the front roller nip line (θ , see Fig. 5), depending on the geometry and parameters adopted during spinning. Some recent innovations in yarn spinning also exhibited purposely or inevitably such a large angle for the improvement of yarn properties [Murrells, Tao, Xu and Cheng, 2009; Tang, Xu and Tao, 2010; Xu, Murrells and Tao, 2008; Xu and Qu, 2001; Xu and Tao, 2003, Xu and Tao, 2008; Xu, Tao and Murrells, 2010; Yang, Tao, Xu and Lam, 2007]. Thus in the present paper, a more generalized theoretical model of ring spinning triangle will be developed using FEM by taking account of the above-mentioned factors ignored previously. With the derivation of the initial conditions and fiber buckling algorithm, the FEM model of spinning triangle will be more close to the practical process.

In the following analysis, the FEM model of spinning triangle will be first developed in Section 2 with the derivations of the initial conditions and the algorithms for fiber buckling effect. In Section 3, numerical simulations are carried out and compared with those by earlier models [Najar, 1996; Hua, Tao, Cheng and Xu, 2007; Bennett and Postle, 1979a, 1979b]. Then, the effect of new spinning parameters such as the inclined spinning triangle and fiber torsional strains will be examined. Finally the conclusions will be given in Section 4.

2 Theoretical analysis

A symmetric geometry model of the spinning triangle is shown in Fig. 5 in which the fibers are uniformly distributed. In this study, the twisted yarn is assumed to have an idealized helical structure with a single fiber core and open packing of circular fibers, giving the yarn with a circular outline (see Fig. 6). It is further assumed that the stress-strain behavior of fibers in ring spinning triangle follows Hooke's law as it is generally agreed [Najar, 1996; Hua, 2006; Hua, Tao, Cheng and Xu, 2007] that it is not beyond the linear region of initial modulus. In addition, the effect of inter-fiber forces is ignored and the fiber ends are twisted together at an imaginary twisting point (O).

2.1 Initial height of spinning triangle

In this analysis, for the geometry relationship shown in Fig. 5, the initial height of spinning triangle H can be expressed in terms of the half of the spinning angle α

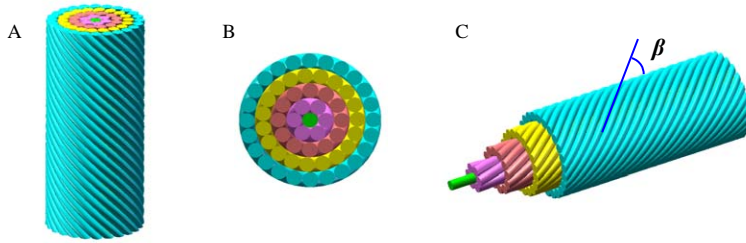


Figure 6: The ideal structure of a yarn (5 layers). (A) a 3D helical structure, (B) a cross-sectional view and (C) a layer structure.

and the width of spinning triangle d :

$$H = \frac{d}{2} \times \frac{1}{\tan \alpha} \tag{1}$$

The width of spinning triangle d is considered as constant and the half of spinning angle α can be formulated in the following way. As shown in Fig. 7, owing to the finite flexural rigidity of the fiber, it has an angle ψ between the line of fiber in spinning triangle and the tangent of the helical fiber in the yarn at the contact point.

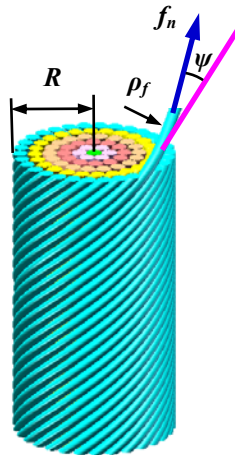


Figure 7: Bending due to flexural rigidity of fiber. R is the yarn radius, ρ_f is the curvature radius of the n th fiber, f_n is the fiber tension of the n th fiber in spinning triangle.

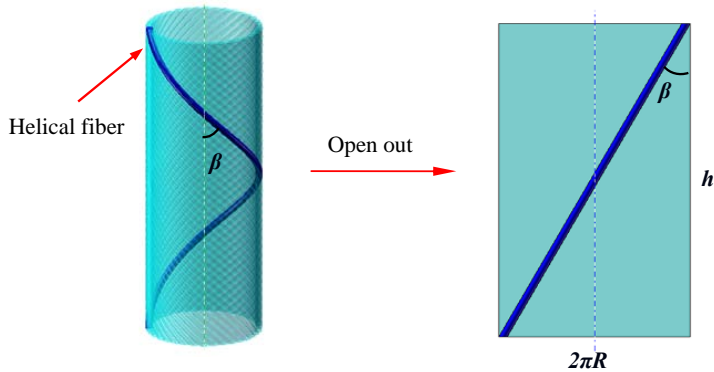


Figure 8: An idealized helical fiber on the surface of yarn. h is the length of one turn of twist.

The relation of the half of spinning angle α and the helix angle β (see Fig. 4 and Fig. 6) of the fiber distributed on the surface of the yarn can be expressed as:

$$\beta = \alpha + \psi \quad (2)$$

As shown in Fig. 7, for an elastic body, the curvature radius ρ_f of the n^{th} fiber is [Grosberg and Plate, 1969]:

$$\frac{1}{\rho_f} = \frac{d\psi}{d\gamma} = 2\sqrt{\frac{f_n}{B}} \sin\left(\frac{\psi}{2}\right) \quad (3)$$

where γ is the distance measured along the line of the fiber, and B is the flexural rigidity of the fiber.

As Emmanuel and Plate (1982) pointed out that the radius ρ_f at the contact point equals the radius of curvature of the helical path of the fiber at this point. Thus:

$$\rho_f = \frac{R}{\sin^2 \alpha} \quad (4)$$

And

$$B = R_f c^2 \quad [\text{Morton and Hearle, 2008}] \quad (5)$$

where R_f is the specific flexural rigidity, yarn linear density $c = \rho\pi R^2$, and ρ is yarn density.

Substituting Eqs. (4) and (5) into the Eq. (3), it follows that:

$$\cos \psi = 1 - \frac{R_f c^2 \sin^4 \alpha}{2 f_n R^2} \quad (6)$$

In the second term $\frac{R_f c^2 \sin^4 \alpha}{2 f_n R^2}$ of Eq. (6), R_f , c and R are constants and the terms vary with α and f_n . In the analysis of low-twist yarns, the bending of fiber can be ignored. Hence, in this study, the helical angle β of the fibers distributed on the surface of the yarn is equal to the half of spinning angle in the initial conditions of this model, as shown in Eq. (7).

$$\psi = 0, \text{ or } \alpha = \beta \quad (7)$$

As shown in Fig. 8, opening the helical yarn out flat, the helix angle of yarn can be expressed as:

$$\tan \beta = 2\pi R/h = 2\pi RT \quad (8)$$

where T is yarn twist expressed by turns per meter (tpm).

Substituting Eqs. (7) and (8) into the Eq. (1), the relation between yarn linear density, yarn twist and the height of spinning triangle can be written as follows:

$$H = \frac{d}{4T} \times \sqrt{\frac{\rho}{c\pi}} \quad (9)$$

Hence the initial height of spinning triangle is largely dependent on the yarn linear density c and yarn twist levels (T).

2.2 Initial strain of fibers

If all the fibers are twisted into the yarn and there is no fiber loss during spinning, the equation of mass conservation can be employed for the spinning triangle:

$$\pi r_1^2 \rho_1 v_1 + \pi r_2^2 \rho_2 v_2 + \dots + \pi r_i^2 \rho_i v_i + \dots + \pi r_n^2 \rho_n v_n = \pi R^2 \rho v_{yarn}, \quad (10)$$

where r_i , ρ_i and v_i are the radius, density and velocity of the i^{th} fiber, respectively, n is the total number of fibers, and v_{yarn} is the velocity of the yarn.

The physical meaning shown in Eq. (10) is that the total mass of fibers entering the spinning triangle per unit time is equal to that of fibers leaving the spinning triangle in the form of yarn per unit time. With the same type of materials, it can be reasonably assumed that, at the entering line (front roller nip line), all the fibers

have the same circular cross section with ideal radius and density, and the fibers are delivered at the same speed:

$$r_1 = r_2 = \cdots = r_n = r, \quad \rho_1 = \rho_2 = \cdots = \rho_n = \rho_0, \quad v_1 = v_2 = \cdots = v_n = v_0 \quad (11)$$

where r , ρ_0 and v_0 are the radius, density and velocity of the fibers, respectively, Substituting Eq. (11) into Eq. (10), we can obtain:

$$n\pi r^2 \rho_0 v_0 = \pi R^2 \rho v_{yarn}. \quad (12)$$

In view of the delivery speed, Eq. (12) can be further written as:

$$\frac{v_0}{v_{yarn}} = \frac{\pi R^2 \rho}{n\pi r^2 \rho_0} = \frac{c}{nc_0} \quad (13)$$

where c_0 is linear density of a single fiber.

In formulation of the initial conditions, fiber initial strain can be considered as a sum of two components. The first component can be understood as a “drafting” result of spinning triangle because of pulling action and it is solely generated by the difference of delivery velocity between fibers and yarn:

$$\varepsilon_0 = \frac{H - L_0}{L_0} = 1 - \frac{v_0}{v_{yarn}} = 1 - \frac{c}{nc_0} \quad (14)$$

where L_0 is the initial length of fibers inside the spinning triangle.

According to Eq. (14), all fibers are equally extended, regardless of their positions in the spinning triangle and the triangle profile of spinning triangle. Then the second component is purely resulted from the triangle profile of spinning triangle:

$$\varepsilon_i = \frac{L_i - H}{H} \quad (15)$$

Therefore the total initial strain of i^{th} fiber in the spinning triangle can be obtained by considering the two components in Eqs. (14) and (15):

$$\varepsilon_i^* = \frac{L_i - L_0}{L_0} = \varepsilon_i + \varepsilon_i \varepsilon_0 + \varepsilon_0 \cong \varepsilon_i + \varepsilon_0 = \frac{L_i - H}{H} + \left(1 - \frac{v_0}{v_{yarn}}\right) \quad (16)$$

In practice, the strain ε_0 in Eq. (16) can be considered as a correction factor and obtained by measuring the total number of fibers, the linear densities of a single fiber and yarn with Eq. (14). In this analysis, it is assumed that the delivery velocities of fiber and yarn are the same (i.e. $v_0 = v_{yarn}$), so the total initial strain of i^{th} fiber (ε_i^*)

in Eq. (16) just equals the fiber strain generated by the triangle profile. To implement the total fiber initial strains formulated in Eq. (16), an initial spinning tension force will be exerted on the twisting point so that the central fiber is straight at zero extension and the other fibers are extended. Under the initial fiber strains, if the actual spinning tension is larger than the initial force, fibers in the spinning triangle will be further elongated, otherwise, they will be contracted or remain unchanged. Some examples of fiber initial strain distribution are shown in Fig. 9. Fig. 9(A) illustrates a contour plot of fiber initial strain for a yarn of 58g/km (linear density unit: grams per 1000m) with a twist level of 398tpm (unit: turns per meter). The fiber initial strain curves under different yarn twists (398tpm, 436tpm, 486tpm, 523tpm) for the same yarn linear density of 58g/km are also shown in Fig. 9(B). As shown in Fig. 9(B), the position of fibers along the front roller nip line (or the width of spinning triangle) is normalized from -0.5 to 0.5 with the central point as zero.

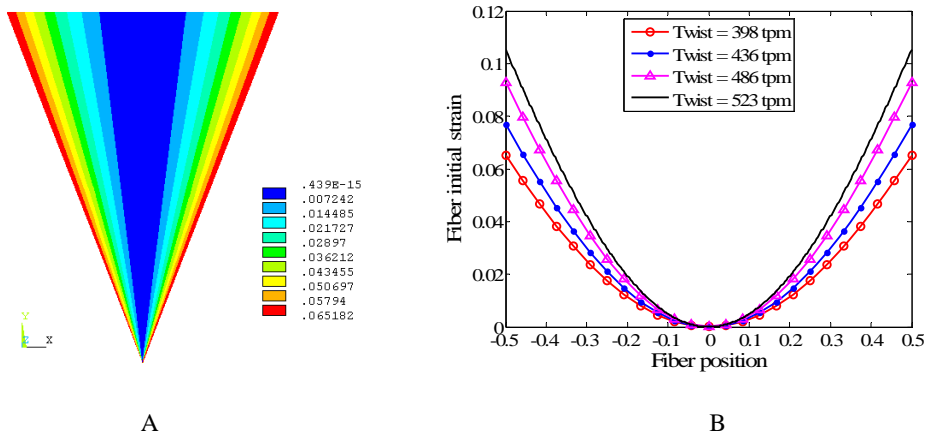


Figure 9: Examples of fiber initial strain (yarn with a linear density of 58g/km). (A) a contour plot of fiber initial strain (yarn twist: 398tpm) and (B) fiber initial strains at different yarn twist levels.

2.3 FEM model of spinning triangle

The constituent fibers in the spinning triangle are considered as 3-D beams with the tensile, compressive, torsional and bending capabilities. In this study, it focuses on analyzing the effects of spinning parameters on the fiber structural and mechanical behavior, therefore the stationary model of spinning triangle will be developed, which is similar to the objectives of previous studies [Najar, 1996; Hua, 2006; Hua,

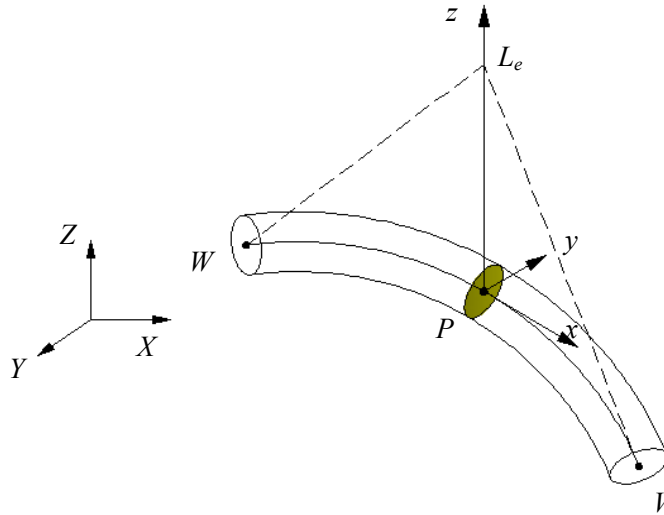


Figure 10: The adopted beam element. W, V, and P are the nodes of the element, L_e is the orientation node, x, y and z are the directions of element coordinate system. The shape functions for the selected 3-D beam element are:

Tao, Cheng and Xu, 2007]. As shown in Figure 5, the governing equations of the fibers in the spinning triangle are:

$$\left\{ \begin{array}{l} \sum_{i=1}^n f_i \cos \alpha_i - F_o \cos \theta = 0 \\ - \sum_{i=1}^{\frac{n-1}{2}} f_i \sin \alpha_i + \sum_{i=\frac{n+1}{2}}^n f_i \sin \alpha_i - F_o \sin \theta = 0 \\ \sum_{i=1}^n m_i \cos \alpha_i + \sum_{i=1}^n R_i f_i \sin \alpha_i - M_o \cos \theta = 0 \\ - \sum_{i=1}^{\frac{n-1}{2}} m_i \sin \alpha_i + \sum_{i=\frac{n+1}{2}}^n m_i \sin \alpha_i - M_o \sin \theta = 0 \\ EA \frac{d\omega_i}{dt_i} - f_i(t_i) = 0 \\ GI_p \frac{d\phi_i}{dt_i} - m_i(t_i) = 0 \end{array} \right. \quad (17)$$

Where R_i is the distance of the i^{th} fiber from the yarn-axis in the yarn cross-section, E is the modulus of elasticity, A is the cross-section area of fiber, GI_p is the torsional rigidity of fiber, ω_i , ϕ_i and t_i are the axial deformation, torsion angle and axial

direction variate of the i^{th} fiber, respectively.

The fibers in spinning triangle are divided into a set of 3-D beam elements based on Timoshenko beam theory and each end node has six degrees of freedom, as shown in Fig. 10.

The shape functions for the selected 3-D beam element are:

$$\begin{cases} \delta = \frac{1}{2}[\delta_W(-s + s^2) + \delta_V(s + s^2) + \delta_P(1 - s^2)] \\ \zeta = \frac{1}{2}[\zeta_W(-s + s^2) + \zeta_V(s + s^2) + \zeta_P(1 - s^2)] \\ \eta = \frac{1}{2}[\eta_W(-s + s^2) + \eta_V(s + s^2) + \eta_P(1 - s^2)] \\ \lambda_x = \frac{1}{2}[\lambda_{xW}(-s + s^2) + \lambda_{xV}(s + s^2) + \lambda_{xP}(1 - s^2)] \\ \lambda_y = \frac{1}{2}[\lambda_{yW}(-s + s^2) + \lambda_{yV}(s + s^2) + \lambda_{yP}(1 - s^2)] \\ \lambda_z = \frac{1}{2}[\lambda_{zW}(-s + s^2) + \lambda_{zV}(s + s^2) + \lambda_{zP}(1 - s^2)] \end{cases} \quad (18)$$

where δ , ζ and η are the translations in the x , y , z directions under the element coordinate system, respectively. λ_x , λ_y or λ_z is the rotational angle about its corresponding direction. s is a normalized coordinate, starting from -1.0 on one side of the element to +1.0 on the other.

The overall stiffness matrix $[K]$ can be obtained by:

$$[K] = \sum_{e=1}^{n_e} [K]^e \quad (19)$$

where n_e is the number of elements, $[K]^e$ is the element stiffness matrix in the global coordinate system.

Thus the static analysis of the FEM model will be a solution of the following equations:

$$[K] \{u\} = \{F\} \quad (20)$$

where $\{u\}$ and $\{F\}$ are assembled nodal displacement and loading vectors, respectively.

The degrees of freedom (DOFs) of the nodes which are on the front roller nip line are all equal to zero, so the displacement boundary condition of the model can be given by:

$$\{u^k\} = \{0\} \quad (21)$$

where k is the node on the front roller nip line.

The spinning tension F_o and spinning torque M_o are applied on the twisting point O , thus the force boundary conditions of the model are as follows:

$$\begin{Bmatrix} f_X^j \\ f_Y^j \\ f_Z^j \\ m_X^j \\ m_Y^j \\ m_Z^j \end{Bmatrix} = \begin{Bmatrix} F_o \sin \theta \\ F_o \cos \theta \\ 0 \\ M_o \sin \theta \\ M_o \cos \theta \\ 0 \end{Bmatrix} \quad (22)$$

where j is the node on the convergence point.

The system of simultaneous linear equations generated by the finite element procedure is solved either using a direct elimination process or an iterative method. In this study, the Sparse Direct Solver was employed. Eq. (20) was solved by triangular decomposition of matrix $[K]$ to yield the following equation:

$$[L][U]\{u\} = \{F\} \quad (23)$$

where $[L]$ is the lower triangular matrix and $[U]$ is the upper triangular matrix.

2.4 Element birth and death for fiber buckling

In the actual spinning process, fiber buckling is a very common phenomenon that occurs in center fibers of spinning triangle, as shown in Fig. 11.

If the fiber is treated as an elastic thin rod under an axial compressive load with both ends clamped, the critical compressive load required to cause fiber buckling is given by [Timoshenko, 1961]:

$$P_{cr} = \frac{4\pi^2 EI}{l_c^2} \quad (24)$$

where I is the moment of inertia of the fiber with a circular cross-section of radius r , and l_c is the clamped length of fiber.

Then, the critical fiber strain beyond which fiber buckling occurs is given as:

$$\epsilon_{cr} = \frac{\pi^2 r^2}{l_c^2} \quad (25)$$

As the small term of ϵ_{cr} is approximately 10^{-6} [Hua, Tao, Cheng and Xu, 2007], the element birth and death condition of the FEM can be employed to deactivate certain elements whose compressive strains are beyond the critical fiber strain. In the

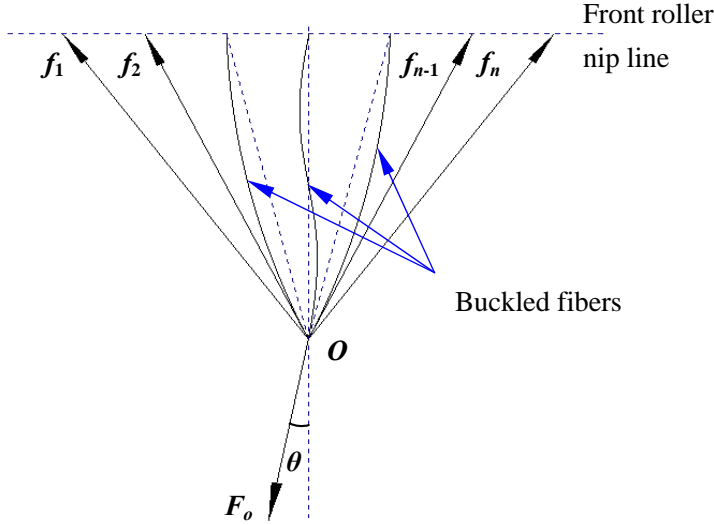


Figure 11: Fiber buckling in spinning triangle

algorithm, a deactivated element physically remains in the model but contributes a near-zero stiffness value $[K]^e$ to the overall matrix of $[K]$ in Eq. (19).

With the above assumptions and deductions, the theoretical model of a symmetric ring spinning triangle using FEM has been developed.

3 Results and discussion

3.1 Fiber tension distribution compared with the energy method

In order to evaluate the validity of the proposed FEM model of spinning triangle, two simulations of fiber tension distribution under different spinning tensions and yarn twists will be carried out in comparison with the results by Najjar (1996) and Hua, Tao, Cheng and Xu (2007) using the energy method. With the same input parameters by Najjar (1996), the simulation results of fiber tension distributions in spinning triangle under different spinning tensions are shown in Fig. 12. It shows that as the spinning tension is increased, the fiber tension at each position of spinning triangle is constantly increased. To compare with the results of symmetric geometry model by Hua, Tao, Cheng and Xu (2007), the simulation results of fiber tension distribution at different yarn twists with fiber buckling considered are shown in Fig. 13. It was noted that the gradient of fiber tension curve becomes steeper and the maximum fiber tension is increased with the increase of yarn twist. Comparing the FEM results with the energy method results by Najjar (1996) and

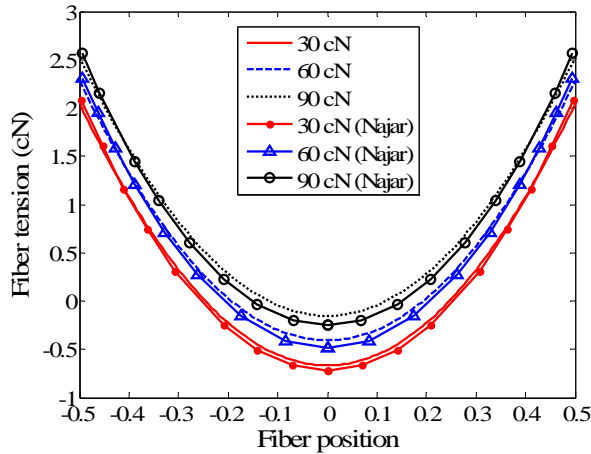


Figure 12: Fiber tensions under different spinning tensions. The twist of 25g/km yarn is 418tpm, spinning tensions are 30cN, 60cN and 90cN.

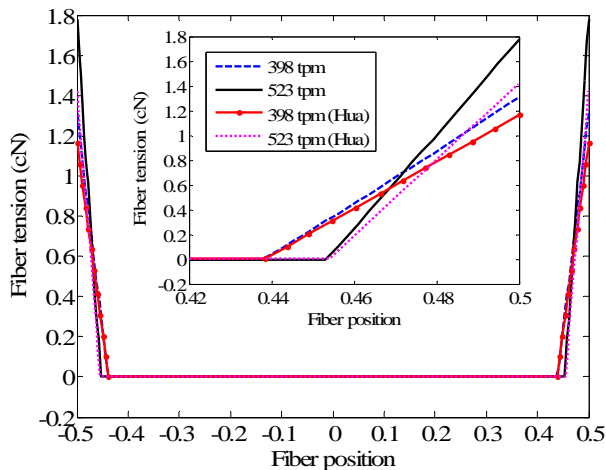


Figure 13: Fiber tensions (with fiber buckling) under different yarn twists. Spinning tension of 58g/km yarn is 30cN, yarn twists are 398tpm and 523tpm.

Hua, Tao, Cheng and Xu (2007), it is noted that the results (both the trend of curves and the numerical values of fiber tension distributions) obtained by the FEM proposed in this paper are in good agreements with previous results by the energy method [Najar, 1996; Hua, Tao, Cheng and Xu, 2007].

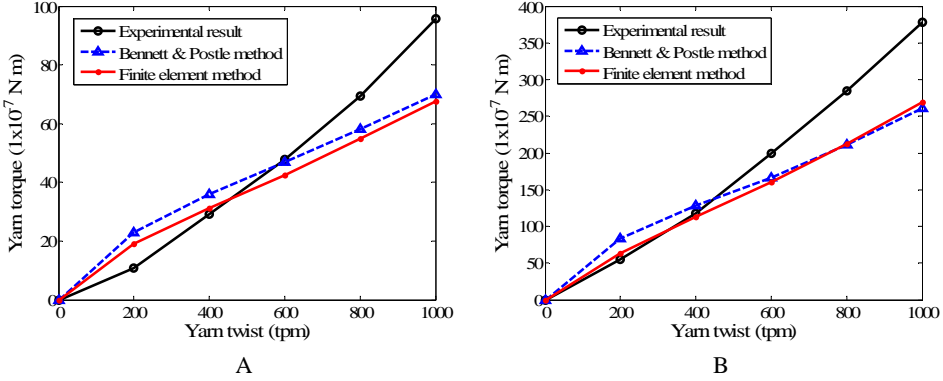


Figure 14: The total yarn torque obtained by the FEM and Bennett & Postle (1979b): (A) the torque of 33g/km yarn and (B) the torque of 68g/km yarn.

3.2 Yarn torque compared with experimental and theoretical results by others

The spinning parameters of two yarns (yarn linear density: 33g/km and 68g/km) will be employed to compare yarn torque obtained by the FEM model with those from earlier experiments and model [Bennett and Postle, 1979a, 1979b]. The yarn torque discussed here is composed of three components, namely the torques generated by fiber tension, fiber bending and fiber torsion [Bennett and Postle, 1979a]:

$$M = M_T + M_B + M_E \quad (26)$$

where M_T is the yarn torque generated by fiber torsional stresses, M_B is the yarn torque generated by fiber bending stresses, and M_E is the yarn torque generated by fiber tensile stresses.

The yarn torque solely generated by the fiber tension can be calculated by considering a discrete distribution of fibers inside yarn [Hua, Tao, Cheng and Xu, 2010]:

$$M_E = \sum_{i=1}^n M_{Ei} = \sum_{i=1}^n f_i R_i \sin \beta_i \quad (27)$$

where M_{Ei} is the component of yarn torque due to i^{th} fiber tension, β_i is the helical angle of the i^{th} fiber within the yarn.

Previous study [Postle, Burton and Chaikin, 1964] showed that the yarn torques generated by fiber bending (M_B) and fiber torsion (M_T) are significantly smaller than the torque by fiber tension (M_E) and thus are ignorable in most cases. In this study, the contribution of fiber bending and torsion to the total yarn torque will

also be included. As the fiber bending and torsion are mainly dependent on the spatial arrangement of fibers inside a yarn and yarn twist, the two components of yarn torque (i.e. M_T and M_B) can be reasonably assumed to be the same in this comparison since an ideal helical yarn structure is adopted in both methods. All the components of yarn torque calculated by Bennett and Postle (1979b) and the current FEM model are listed in Tab. 1.

Fig. 14 shows the results of total yarn torque obtained by the FEM model together with Bennett & Postle's theoretical results and experimental measurements [Bennett and Postle, 1979b]. In Fig. 14(A) (33g/km yarn), the theoretical torques obtained by the FEM are in better agreements with the experimental measurements than Bennett's theoretical results below the twist level of 500tpm, while the situation becomes reverse in the twist range of 500-1000 tpm. From the developing trend of the curve, the result of this study is expected to be more close to the experimental measurements at the twist levels greater than 1000tpm. In Fig. 14(B) (68g/km yarn), it is noted that the results of this study are generally in better agreements with the experimental measurements than Bennett & Postle's theoretical calculations in the whole range of yarn twists except between 400 and 600 tpm.

3.3 The effect of new parameters on fiber tension and torsion distributions

Using the developed FEM model, the effects of the inclined spinning angle and fiber torsional strains which were ignored previously, can be evaluated. The parameters in the analysis were: yarn linear density of 25g/km, yarn twist of 418tpm, spinning tension of 30cN, and the angles (θ) between yarn spinning tension and the vertical axis of the nip line is assumed as 10° . The simulation results are shown in Fig. 15.

As seen in Fig. 15(A), with the inclined spinning angle θ , the fibers which are located on the right side of spinning triangle (i.e. the side opposite to the direction of spinning tension) are subject to larger tensile loadings than the fibers on the other side. For fiber torsional strains shown in Fig. 15(B), the fibers distributed in the center of spinning triangle are subject to the largest torsional deformation and the magnitudes of fiber torsion is gradually reduced from the center to both sides of spinning triangle.

4 Conclusions

In this paper, FEM has been applied in the theoretical modeling of the spinning triangle in order to develop a generalized theoretical model and address more complicated yarn formation process. The initial strain of fibers and the algorithm of element birth and death were employed with consideration of the inclined spinning tension and fiber torsional strains. With the involvement of more influential facts

Table 1: The spinning parameters and calculated components of yarn torque

Yarn linear density (g/km)	Number of fibers	Spinning tension (cN)	Yarn Twist (tpm)	M_T ($\times 10^{-7}$ N m)	M_B ($\times 10^{-7}$ N m)	M_E	
						by Bennett & Postle ($\times 10^{-7}$ N m)	by FEM ($\times 10^{-7}$ N m)
33	61	3.5	200	15	0	8	4
			400	21	2	13	8
			600	23	7	17	12
			800	25	13	20	17
			1000	26	20	24	22
68	127	11.5	200	31	2	50	30
			400	43	9	76	61
			600	46	21	99	93
			800	47	39	125	127
			1000	48	59	154	162

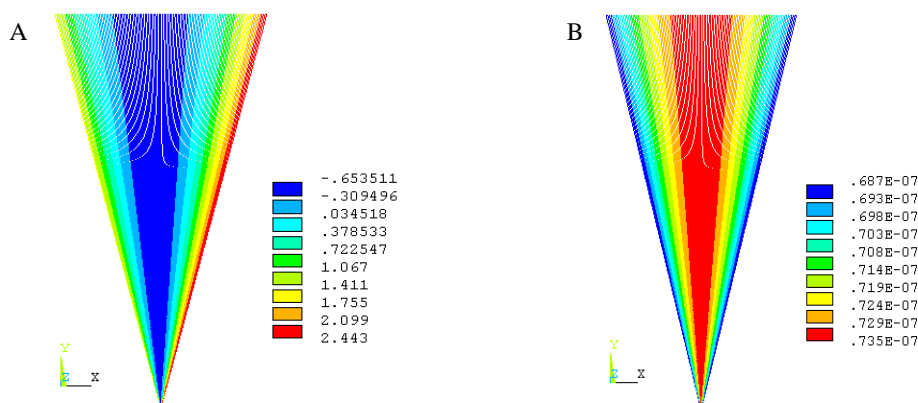


Figure 15: Fiber mechanical behavior considering the inclined angle of spinning tension: (A) a contour plot of fiber tension (unit: cN) and (B) a contour plot of fiber torsion (unit: N m).

in the theoretical model, the results will be more accurate and meaningful.

Numerical results were presented and compared with those by earlier models. The comparative studies showed that the predictions by the developed FEM model were in good agreements with those by Najar (1996) and Hua, Tao, Cheng and Xu (2007) using the energy method. In addition, the yarn torques obtained by the FEM model were generally more close to the experimental measurements compared with those by Bennett and Postle (1979b). With this FEM model, numerical simulations were also carried out to evaluate the effect of new spinning parameters ignored previously on the mechanical performance of spinning triangle.

Acknowledgement: The authors wish to acknowledge the funding support from the Hong Kong Polytechnic University. S.Y. Li would also like to thank the Hong Kong Polytechnic University for providing her with a postgraduate scholarship.

References

Bennett, J. M.; Postle, R. (1979a): A Study of Yarn Torque and Its Dependence on the Distribution of Fiber Tensile Stress in the Yarn. 1. Theoretical Analysis. *Journal of the Textile Institute*, vol. 70, pp. 121-132.

Bennett, J. M.; Postle, R. (1979b): A Study of Yarn Torque and Its Dependence on the Distribution of Fiber Tensile Stress in the Yarn. 2. Experimental. *Journal of the Textile Institute*, vol. 70, pp. 133-141.

Bouzidi, R.; Ravaut, Y.; Wielgosz, C. (2003): Finite Elements for 2D Problems of Pressurized Membranes. *Computers & Structures*, vol. 8, pp. 2479-2490.

Cartaud, F.; Touze-Foltz, N.; Duval, Y. (2005): Experimental Investigation of the Influence of a Geotextile Beneath the Geomembrane in a Composite Liner on the Leakage Through a Hole in the Geomembrane. *Geotextiles and Geomembranes*, vol. 23, pp. 117-143.

Duan, Y.; Keefe, M.; Bogetti, T. A.; Powers, B. (2006): Finite Element Modeling of Transverse Impact on a Ballistic Fabric. *International Journal of Mechanical Sciences*, vol. 48, pp. 33-43.

El-Shiekh, A. (1965): On the Mechanics of Twist Insertion. *Ph.D. dissertation*. Massachusetts Institute of Technology, Massachusetts, USA.

Emmanuel, A.; Plate, D. E. A. (1982): An Alternative Approach to Two-fold Weaving Yarn. Part II: the Theoretical Model. *Journal of the Textile Institute*, vol. 73, pp. 107-116.

Fujino, K.; Uno, M.; Shiomi, A.; Yanggawa, Y.; Kitada, Y. (1962): A Study on the Twist Irregularity of Yarn Spun on the Ring Spinning Frame. *Journal of the Textile Machinery Society of Japan*, vol. 8, pp. 51-62.

Grosberg, P.; Plate, D. E. A. (1969): Capstan Friction for Polymer Monofilaments with Rigidity. *Journal of the Textile Institute*, vol. 60, pp. 268-283.

Hearle, J. W. S.; Grosberg, P.; Backer, S. (1969): *Structural Mechanics of Fibers, Yarns, and Fabrics*. New York: Wiley-Interscience.

Hua, T. (2006): Production, Properties and Structures of Short Staple Low Torque Singles Ring Yarn for Weaving. *Ph.D. dissertation*. The Hong Kong Polytechnic University, Hong Kong.

Hua, T.; Tao, X. M.; Cheng, K. P. S.; Xu, B. G. (2007): Effects of Geometry of Ring Spinning Triangle on Yarn Torque Part I: Analysis of Fiber Tension Distribution. *Textile Research Journal*, vol. 77, pp. 853-863.

Hua, T.; Tao, X. M.; Cheng, S.; Xu, B. G. (2010): Effects of Geometry of Ring Spinning Triangle on Yarn Torque Part II: Distribution of Fiber Tension within a Yarn and its Effects on Yarn Residual Torque. *Textile Research Journal*, vol. 80, pp. 116-123.

Jiang, K.; Li, Q.; Fan, S. (2002): Nanotechnology: Spinning Continuous Carbon Nanotube Yarns. *Nature*, vol. 419, pp. 801-801.

Krause, H. W.; Soliman, H. A.; Tian, J. L. (1991): Investigation of the Strength of the Spinning Triangle in Ring Spinning. *Melliand Textilberichte*, vol. 72, pp. 499-502.

Liu, Y.; Hu, H.; Lam, J. K. C.; Liu, S. (2010): Negative Poisson's Ratio Weft-

knitted Fabrics. *Textile Research Journal*, vol. 80, pp. 856-863.

Miller, W.; Hook, P. B.; Smith, C. W.; Wang, X.; Evans, K. E. (2009): The Manufacture and Characterisation of a Novel, Low Modulus, Negative Poisson's Ratio Composite. *Composites Science and Technology*, vol. 69, pp. 651-655.

Morton, W. E.; Hearle, J. W. S. (2008): *Physical Properties of Textile Fibres*. Cambridge, Textile Institute, Woodhead Pub., Boca Raton, Fla..

Murrells, C. M.; Tao, X. M.; Xu, B. G.; Cheng, K. P. S. (2009): An Artificial Neural Network Model for the Prediction of Spirality of Fully Relaxed Single Jersey Fabrics. *Textile Research Journal*, vol. 79, pp. 227-234.

Najar, S. S. (1996): An Analysis of the Twist Triangle in Ring Spinning. *Ph.D. dissertation*. University of New South Wales, Australia.

Oñate, E.; Kröplin, B. (2005). *Textile Composites and Inflatable Structures*. Berlin, London: Springer.

Pavlov, Y. V. (1965): Structural Transformations in the Fiber Assembly at the Twist Threshold at the Instant of Rupture. *Technology of the textile industry U.S.S.R.*, vol. 4, pp. 57-63.

Postle, R.; Burton, P.; Chaikin, M. (1964): The Torque in Twisted Singles Yarns. *Journal of the Textile Institute*, pp. 448-461.

Quek, S. C.; Waas, A. M.; Shahwan, K. W.; Agaram, V. (2003): Analysis of 2D Triaxial Flat Braided Textile Composites. *International Journal of Mechanical Sciences*, vol. 45, pp. 1077-1096.

Sejnoha, M.; Zemana, J. (2008): Micromechanical Modeling of Imperfect Textile Composites, *International Journal of Engineering Science*, vol. 46, pp. 513-526.

Smit, E.; Buttner, U.; Sanderson, R. D. (2005): Continuous Yarns from Electrospun Fibers. *Polymer*, vol. 46, pp. 2419-2423.

Sze, K. Y.; Liu, X. H. (2007): Fabric Drape Simulation by Solid-shell Finite Element Method. *Finite Elements in Analysis and Design*, vol. 43, pp. 819-838.

Tabiei, A.; Jiang, Y. (1999): Woven Fabric Composite Material Model with Material Nonlinearity for Nonlinear Finite Element Simulation. *International Journal of Solids and Structures*, vol. 36, pp. 2757-2771.

Tanaka, M.; Noguchi, H.; Fujikawa, M.; Sato, M.; Oi, S.; Kobayashi, T.; Furuchi, K.; Ishimaru, S.; Nonomura, C. (2010): Development of Large Strain Shell Elements for Woven Fabrics with Application to Clothing Pressure Distribution Problem. *CMES: Computer Modeling in Engineering & Sciences*, vol. 62, pp. 265-290.

Tang, H. B.; Xu, B. G.; Tao, X.M. (2010): A New Analytical Solution of the

Twist Wave Propagation Equation with Its Application in a Modified Ring Spinning System. *Textile Research Journal*, vol. 80, pp. 636-641.

Timoshenko, S. P. (1961): *Theory of Elastic Stability*. New York: McGraw-Hill.

Wang, L.; Zhang, S.; Gao, W. M.; Wang, X. (2007): FEM Analysis of Knife Penetration through Woven Fabrics. *CMES: Computer Modeling in Engineering & Sciences*, vol. 20, pp. 11-20.

Xu, B. G.; Murrells, C. M.; Tao, X. M. (2008): Automatic Measurement and Recognition of Yarn Snarls by Digital Image and Signal Processing Methods. *Textile Research Journal*, vol. 78, pp. 439-456.

Xu, B. G.; Qu, L.S. (2001): A New Practical Modal Method for Rotor Balancing. *Proceedings of the Institution of Mechanical Engineers Part C-Journal of Mechanical Engineering Science*, vol. 215, pp. 179-189.

Xu, B. G.; Tao, X. M. (2003): Integrated Approach to Dynamic Analysis of Yarn Twist Distribution in Rotor Spinning Part I: Steady State. *Textile Research Journal*, vol. 73, pp. 79-89.

Xu, B. G.; Tao, X. M. (2008): Techniques for Torque Modification of Singles Ring Spun Yarns. *Textile Research Journal*, vol. 78, pp. 869-879.

Xu, B. G.; Tao, X. M.; Murrells, C. M. (2010): Evaluation of a Digital Image-signal Approach on the Automatic Measurement of Cotton Yarn Snarls. *Textile Research Journal*, vol. 80, pp. 1151-1159.

Yang, K.; Tao, X. M.; Xu, B. G.; Lam, J. (2007): Structure and Properties of Low Twist Short-staple Singles Ring Spun Yarns. *Textile Research Journal*, vol. 77, pp. 675-685.

Zakhidov, A. L. A.; Nanjundaswamy, R.; Obratsov, A. N.; Zhang, M.; Fang, S.; Klesch, V. I.; Baughman, R. H.; Zakhidov, A. A. (2007): Field Emission of Electrons by Carbon Nanotube Twist-yarns. *Applied Physics A*, vol. 88, pp. 593-600.

Zhang, M.; Atkinson, K. R.; Baughman, R. H. (2004): Multifunctional Carbon Nanotube Yarns by Downsizing an Ancient Technology. *Science*, vol. 306, pp. 1358-1361.

Zhang, Y. T.; Liu, C. Y.; Du, R. X. (2007): Buckling Analysis of Plain Knitted Fabric Sheets under Simple Shear in an Arbitrary Direction. *International Journal of Solids and Structures*, vol. 44, pp. 7049-7060.

